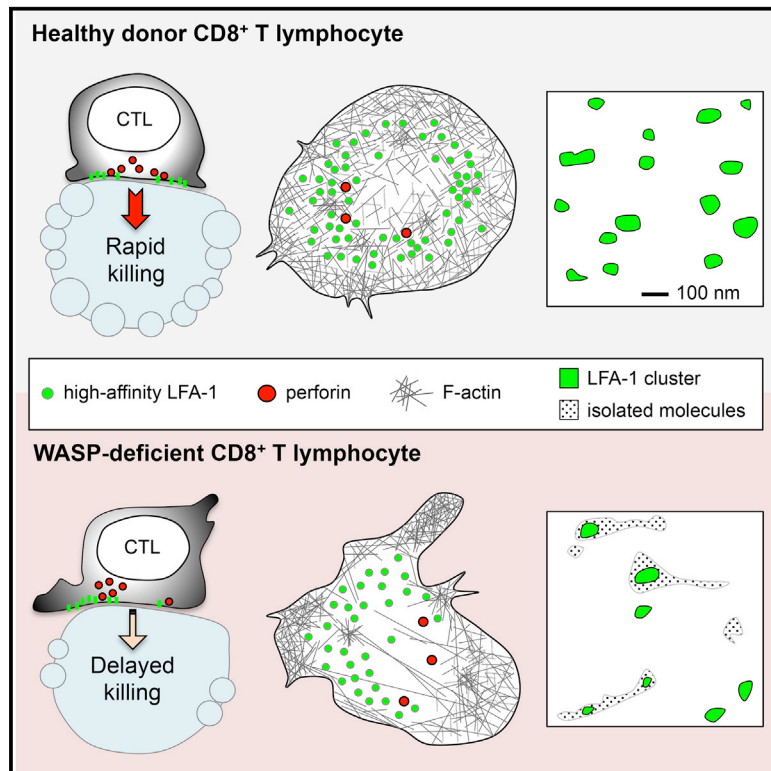


## The Wiskott-Aldrich Syndrome Protein Contributes to the Assembly of the LFA-1 Nanocluster Belt at the Lytic Synapse

### Graphical Abstract



### Authors

Raïssa Houmadi, Delphine Guipouy, Javier Rey-Barroso, ..., Salvatore Valitutti, Sophie Allart, Loïc Dupré

### Correspondence

loic.dupre@inserm.fr

### In Brief

A hallmark of the synapse between cytotoxic T cells and target cells is the assembly of an LFA-1 ring. Using super-resolution microscopy approaches, Houmadi et al. report that the LFA-1 ring is composed of nanoclusters embedded in the actin cytoskeleton and identify the pivotal role of WASP in LFA-1 topography.

### Highlights

- High-affinity LFA-1 is organized into a nanocluster belt at the CD8<sup>+</sup> T cell synapse
- LFA-1 nanoclusters locate in the interstices of the actin cytoskeleton meshwork
- WASP controls LFA-1 organization into individual nanoclusters and cluster belt



# The Wiskott-Aldrich Syndrome Protein Contributes to the Assembly of the LFA-1 Nanocluster Belt at the Lytic Synapse

Raïssa Houmadi,<sup>1,2,3,8</sup> Delphine Guipouy,<sup>1,2,3,4,8</sup> Javier Rey-Barroso,<sup>1,2,3</sup> Zilton Vasconcelos,<sup>5</sup> Julie Cornet,<sup>2,6</sup> Manoel Manghi,<sup>2,6</sup> Nicolas Destainville,<sup>2,6</sup> Salvatore Valitutti,<sup>1,2,3,7</sup> Sophie Allart,<sup>1,2,3</sup> and Loïc Dupré<sup>1,2,3,9,\*</sup>

<sup>1</sup>INSERM, UMR 1043, Centre de Physiopathologie de Toulouse Purpan, Toulouse, France

<sup>2</sup>Université Toulouse III Paul Sabatier, Toulouse, France

<sup>3</sup>CNRS, UMR 5282, Toulouse, France

<sup>4</sup>TxCell, Allée de la Nertière, Valbonne, Sophia-Antipolis, France

<sup>5</sup>Fernandes Figueira Institute, Fiocruz, Rio de Janeiro, Brazil

<sup>6</sup>CNRS, UMR 5152, Institut de Recherche sur les Systèmes Atomiques et Moléculaires Complexes, Laboratoire de Physique Théorique, Toulouse, France

<sup>7</sup>Department of Pathology, Institut Universitaire du Cancer-Oncopole de Toulouse, Toulouse, France

<sup>8</sup>These authors contributed equally

<sup>9</sup>Lead Contact

\*Correspondence: [loic.dupre@inserm.fr](mailto:loic.dupre@inserm.fr)

<https://doi.org/10.1016/j.celrep.2017.12.088>

## SUMMARY

T lymphocyte cytotoxicity relies on a synaptic ring of lymphocyte function-associated antigen 1 (LFA-1), which permits polarized delivery of lytic granules. How LFA-1 organization is controlled by underlying actin cytoskeleton dynamics is poorly understood. Here, we explored the contribution of the actin cytoskeleton regulator WASP to the topography of LFA-1 using a combination of microscopy modalities. We uncover that the reduced cytotoxicity of Wiskott-Aldrich syndrome patient-derived CD8<sup>+</sup> T lymphocytes lacking WASP is associated with reduced LFA-1 activation, unstable synapse, and delayed lethal hit. At the nanometric scale, WASP constrains high-affinity LFA-1 into dense nanoclusters located in actin meshwork interstices. At the cellular scale, WASP is required for the assembly of a radial belt composed of hundreds of LFA-1 nanoclusters and for lytic granule docking within this belt. Our study unravels the nanoscale topography of LFA-1 at the lytic synapse and identifies WASP as a molecule controlling individual LFA-1 cluster density and LFA-1 nanocluster belt integrity.

## INTRODUCTION

The integrin lymphocyte function-associated antigen 1 (LFA-1) was initially identified in a screen of antibodies that blocked the lytic activity of CD8<sup>+</sup> cytotoxic T lymphocytes (CTLs) (Davignon et al., 1981). In these cells, LFA-1 is required both for the conjugation with antigen-presenting cells and for the confined delivery of cytotoxic molecules. Indeed, CTL lytic granules are delivered in a secretory domain lying between the center of the synapse enriched in signaling molecules and a peripheral ring of LFA-1

(Stinchcombe et al., 2001). In agreement with the requirement to confine lytic granule delivery with high fidelity, CD8<sup>+</sup> T cells have been shown to form 5-fold more LFA-1 ring junctions than CD4<sup>+</sup> T cells (Somersalo et al., 2004). In the context of the T cell immunological synapse, LFA-1 clusters accumulate over time at the inner side of the lamellar actin network to form a peripheral ring (Anikeeva et al., 2005; Yi et al., 2012). The lateral force provided by the actin retrograde flow has been hypothesized to drive integrin activation by separating  $\alpha$ - and  $\beta$ -integrin cytoplasmic tails (Zhu et al., 2008). In accordance, LFA-1 under the extended conformation localizes to the synapse outer ring, while the open conformation is enriched in a more central ring (Comrie et al., 2015). Initial analysis of LFA-1 topography at the surface of T cells has provided the view that LFA-1 activation results from the assembly of micrometer-scale domains (Kaizuka et al., 2007). However, recent super-resolution microscopy approaches have revealed that LFA-1, instead, assembles into nanometer-scale clusters (Baumgart et al., 2016; Murugesan et al., 2016). The mechanisms that control the organization of LFA-1 into a ring-like structure and that confine LFA-1 into nanoclusters remain to be elucidated.

In this work, we tested the hypothesis that the Wiskott-Aldrich syndrome protein (WASP) might be a major player in the control of LFA-1 activation and organization in CTLs. WASP is a hematopoietic-specific actin cytoskeleton regulator that sets immunological synapse stability and T cell receptor (TCR) activation threshold in CD4<sup>+</sup> T cells (Calvez et al., 2011; Dupré et al., 2002; Sims et al., 2007). Whether it controls the stability of the lytic synapse and whether this might explain its reported role in CTL killing activity (De Meester et al., 2010; Lang et al., 2013) remain unexplored. To test the role of WASP in lytic synapse organization, we investigated actin cytoskeleton ultrastructure and dynamics together with LFA-1 topography in patient-derived WASP-deficient CTLs, using a combination of microscopy tools, including the super-resolution approaches direct stochastic optical reconstruction microscopy (dSTORM) (Heilemann et al., 2008; van de Linde et al., 2011) and structured illumination microscopy (SIM) (Gustafsson, 2000). Our data reveal that WAS CTLs display



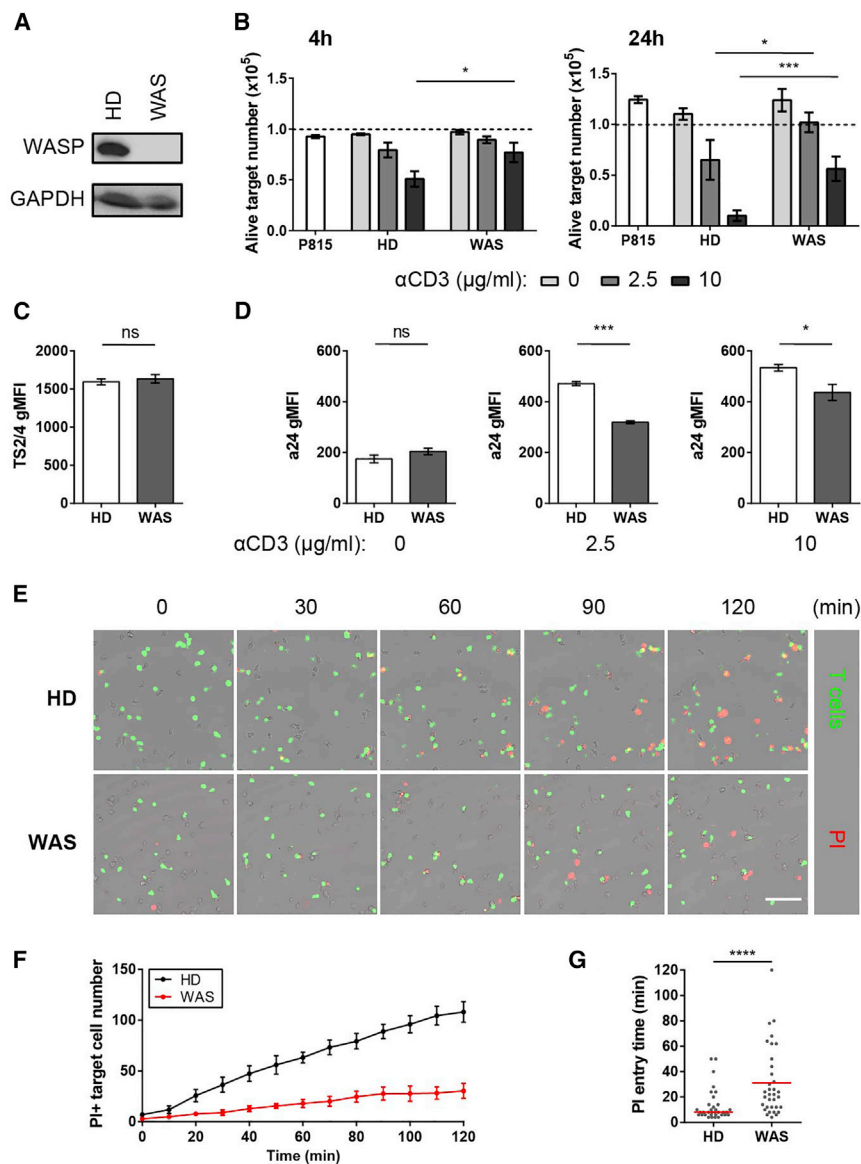


**Figure 1. Reduced Killing Activity and LFA-1 Activation in WASP-Deficient CD8<sup>+</sup> T Cells**

(A) Western blot analysis of WASP expression in CTLs from a healthy donor (HD) and a WAS patient (WAS).

(B) Number of residual alive target cells after 4 and 24 hr of a redirected killing assay at a 2:1 effector:target (E:T) ratio against P815 cells pre-coated with the indicated concentrations of anti-CD3 Ab. Dotted bars represent the reference number of target cells (mean  $\pm$  SEM of 3 independent experiments).

(C) Total LFA-1 expression (TS2/4 Ab) in primary CTLs from 4 HD and 3 WAS patients.

(D) CTLs were co-incubated during 60 min with P815 cells and analyzed for expression of high-affinity LFA-1 (a24 Ab).

(E) Anti-CD3 Ab pre-coated target cells were seeded in the presence of HD or WAS CTLs (green) at a 2:1 E:T ratio. PI (red) was used to track lethal hit delivery. Scale bar, 100  $\mu$ m.

(F) Number of PI-positive target cells along time.

(G) Time delay between the contact of target cells with a CTL and PI entry. 34 conjugates were analyzed for both HD and WAS CTLs.

Graphs indicate mean values  $\pm$  SEM. Statistical significances were obtained with two-tailed Mann-Whitney non-parametric t tests. ns,  $p > 0.05$ ; \* $0.01 < p < 0.05$ ; \*\* $0.001 < p < 0.01$ ; \*\*\* $p < 0.001$ ; \*\*\*\* $p < 0.0001$ .

See also [Figure S1](#), [Movie S1](#), and [Movie S2](#).

reduced LFA-1 activation, non-radial spreading of the lytic synapse, delayed lethal hit delivery, and reduced target cell killing. We further identify that open-conformation LFA-1 nanoclusters are confined into actin meshwork interstices and that such clusters display reduced density in WASP-deficient CTLs. At the cellular scale, WAS CTLs display defects in LFA-1 cluster belt assembly and lytic granule positioning. In conclusion, our study identifies WASP as a key regulator of LFA-1 nanoscale topography in the context of CD8<sup>+</sup> T cell cytotoxic activity.

## RESULTS

### Decreased Killing Potential and Reduced LFA-1 Activation in WAS CD8<sup>+</sup> T Cells

The mechanism underlying the reduced ability of CD8<sup>+</sup> T cells from Wiskott-Aldrich syndrome (WAS) patients to kill target cells

rapidly eliminate P815 target cells, as well as to sustain prolonged killing activity, was reduced ([Figures 1B](#) and [S1E](#)). We then tested whether WASP deficiency might affect LFA-1 activation by measuring the expression of total and open LFA-1 conformations by flow cytometry ([Theorell et al., 2011](#)). The CTLs from the healthy donors and the WAS patients expressed basally comparable levels of total LFA-1 ([Figure 1C](#)). They expressed similar levels of LFA-1 under the open conformation when facing uncoated target cells. However, upon encounter with the anti-CD3 antibody (Ab)-coated target cells, the WASP-deficient CTLs displayed a reduced capacity to upregulate active LFA-1 ([Figure 1D](#)). We then sought to explore whether this reduced LFA-1 activation would be mirrored by abnormal dynamics of CTLs to target cell contacts in the context of killing. Real-time imaging of CTLs and anti-CD3 Ab-coated target cell mixtures shows that, although WASP-deficient CTLs were highly motile

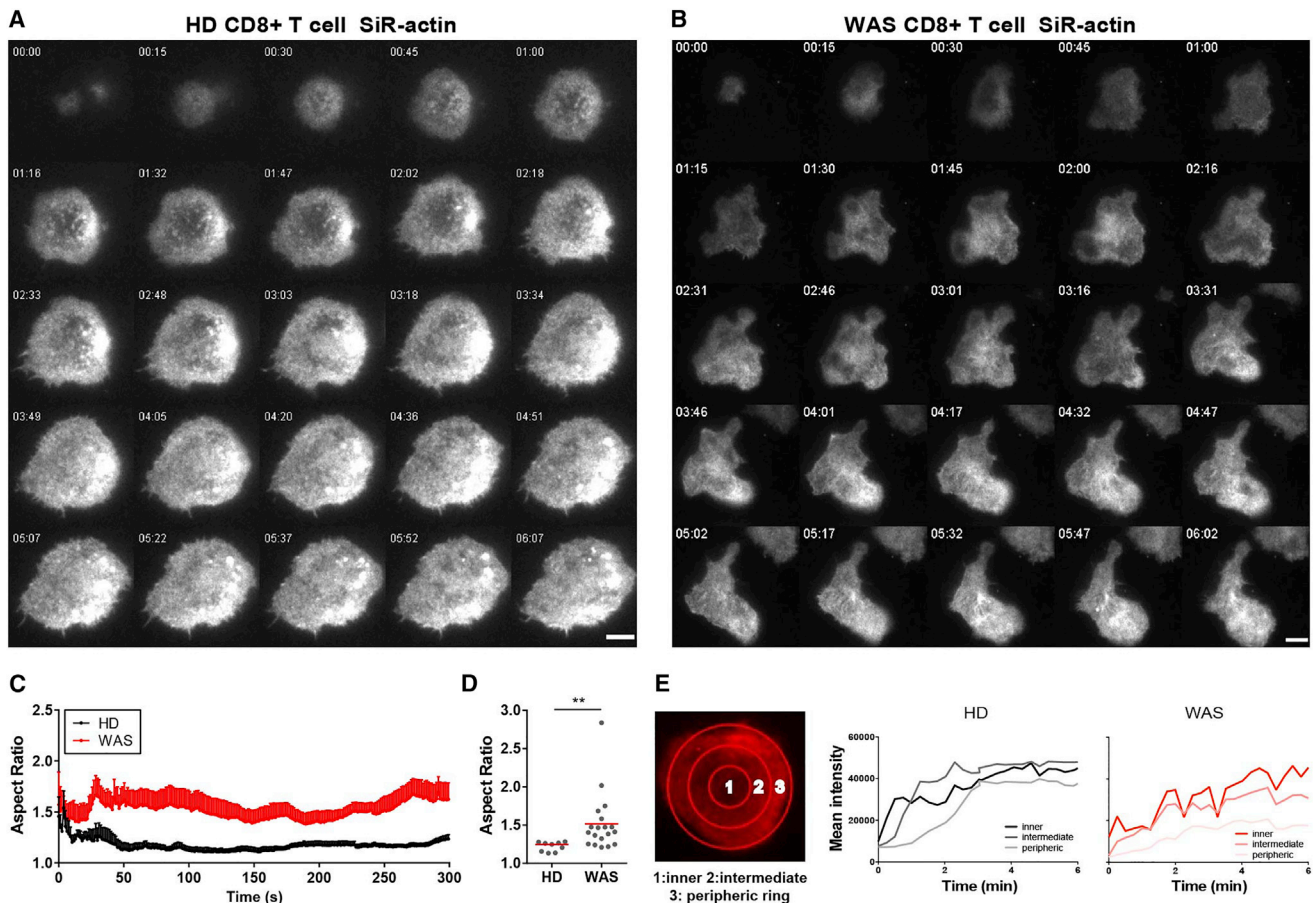


**Figure 2. Abnormal Synapse Shape and F-Actin Dynamics in WAS CD8<sup>+</sup> T Cells**

(A) TIRFM imaging of F-actin dynamics at the contact of a representative healthy donor (HD) CTL adhering to an ICAM-1/anti-CD3-coated surface. Scale bar, 5  $\mu$ m.

(B) TIRFM imaging of a representative WAS patient CTL, imaged as described in (A). Scale bar, 5  $\mu$ m.

(C) Time course of the aspect ratio measured for 6 HD and 6 WAS CD8<sup>+</sup> T cells adhering to an ICAM-1/anti-CD3-coated surface.

(D) Mean aspect ratio of the cells analyzed in (C).

(E) SiR-actin intensity was measured along the time in the 3 indicated concentric circles. This approach was applied to the representative cells displayed in (A) and (B).

Statistical significances were obtained with a two-tailed Mann-Whitney non-parametric t test. \*\*0.001 < p < 0.01.

See also [Figure S2](#).

and able to encounter target cells, killing efficiency was reduced compared to that of control CTLs ([Figure 1E](#); [Movies S1](#) and [S2](#)). The reduced ability of WAS CTLs to kill targets over time ([Figure 1F](#)) was related to an increased delay between initial contact and lethal hit delivery ([Figure 1G](#)). Together, these results indicate that the reduced efficiency of WAS CTLs to eliminate target cells is associated with a delayed lethal hit delivery and a reduced LFA-1 activation.

### Aberrant Actin Cytoskeleton Dynamics and Non-radial Spreading in WAS CD8<sup>+</sup> T Cells

Although WASP deficiency has been reported to distort synapse morphology in primary human T cells ([Calvez et al., 2011](#)), its effect on actin dynamics at the immunological synapse remains to be characterized. For this purpose, we used the cell-permeant SiR-actin dye ([Lukinavičius et al., 2014](#)) to

record F-actin dynamics by total internal reflection fluorescence microscopy (TIRFM), which allows a focus on the cell portion that lays at the immediate contact with the ICAM-1/anti-CD3-coated surface. As shown in a representative healthy donor CD8<sup>+</sup> T cell, spreading occurred within 2 to 3 min and was characterized by a surrounding lamellipodium, shown in the transmitted images ([Figure S2A](#)) and a dense actin meshwork ([Figure 2A](#)). This network was not uniform, since areas of reduced actin density were present toward the center of the synapse, while small actin patches were distributed all over the contact surface. Although the F-actin meshwork was highly dynamical at the synaptic plane, the cell shape did not evolve beyond 3 min. In contrast, the WAS CTL displayed a reduced spreading area and lobular morphology, characterized by nascent lamellipodia on different sides of the cell ([Figure S2B](#)). The WAS cell displayed a variable actin density

along the considered observation time. Intermittently, areas of high intensity fluorescence were observed in the middle of the synapse, out of which actin cables appeared to emerge (Figure 2B). The time course of the aspect ratio (AR) indicated that healthy donor (HD) cells rapidly assembled a circular synapse with an AR value evolving from 1.6 to 1 during the first minute (Figure 2C). However, WAS CTLs were unable to spread radially, as confirmed by AR variations ranging from 1.5 to 1.8 along the observation period. The mean AR of 9 HD and 19 WAS cells confirmed the non-circular morphology of WAS T cell synapses (Figure 2D). To then assess F-actin dynamics during the initial phase of cell spreading, SiR-actin fluorescence intensity was quantified in concentric circles centered on the cell centroid (Figure 2E). In control T cells, F-actin intensity increased sharply over the first 2 min of contact at the center of the synapse and then in the intermediate and peripheral rings, indicating concomitant F-actin polymerization and spreading (Figures 2E and S2C). After 2 min, the intensity of F-actin stabilized, with the highest intensity being measured at the intermediate ring. In contrast, WAS T cells failed to show this biphasic behavior and displayed a more progressive increase in SiR-actin staining over the 6-min observation period. Furthermore, WAS T cells displayed relatively more polymerized actin at the synapse center than at the intermediate ring, and the central F-actin pool displayed high intensity fluctuations. In conclusion, the TIRFM study of F-actin dynamics in WAS CTLs reveals a major defect in actin meshwork organization combined with the inability to spread radially and to establish a stable synapse.

### Biased Distribution of LFA-1 Clusters in WAS T Cells

We implemented a SIM approach to precisely locate active LFA-1 at the CTL synapse and elucidate how it interacts with the actin cytoskeleton meshwork. We also applied this approach to the WAS CTL to understand which precise actin cytoskeleton aberrations might be related to the LFA-1 activation defects identified in these cells. The representative normal CTL depicted in Figure 3A displayed an extended synaptic spreading, with F-actin being enriched both at the periphery, as a thin lamellipodium, and within patches located toward the inner parts of the synapse. Active LFA-1 distributed as very distinct clusters organized into a belt-like structure lying inward to the external F-actin area. Active LFA-1 clusters appeared to be positioned in the interstices of the actin cytoskeleton meshwork. This applied to both the actin-rich area corresponding to the LFA-1 ring and to the actin-poor areas toward the synapse center (Figure 3A, zooms on the right panels). Sections along the z axis showed that the inner part of LFA-1 clusters localized to thin interstices of reduced F-actin density (Figure 3A, central lower panels), suggesting that LFA-1 nanoclusters are confined into the alveoli of the actin cytoskeleton meshwork. Parallel examination of a representative WAS CTL (Figure 3B) revealed that it spread over a reduced area. Although a very rich actin cytoskeleton meshwork composed of highly branched and spiky structures had assembled at the WAS T cell periphery, the synapse center was almost devoid of detectable actin structures. In this cell, active LFA-1 could be detected, but they failed to assemble into a belt. At the ultrastructure level, the most external LFA-1

clusters were positioned in the interstices of the very dense actin cytoskeleton meshwork, while LFA-1 clusters localizing toward the synapse center appeared to not be connected to actin filaments and to distribute less evenly than in the control cell (Figure 3B, zooms on the right panels). Sections along the z axis of the WAS CTL confirmed both the asymmetry of the LFA-1 ring and the biased distribution of LFA-1 clusters in relationship with the actin meshwork (Figure 3B, central lower panels). The partial decorrelation of active LFA-1 clusters from the areas of enriched actin density and the asymmetry of the WAS CTL was highlighted by an analysis of LFA-1 and F-actin intensity profiles within cell quadrants. In control cells, active LFA-1 was highly enriched at 8  $\mu\text{m}$  from the cell center, with a slight inner shift as compared to the peripheral F-actin-rich area (Figure 3C). In those cells, LFA-1 distributed evenly among the areas enriched in F-actin (IN) and those devoid of F-actin (OUT) (Experimental Procedures) (Figure 3D). This distribution is probably attributable to the fact that, although LFA-1 clusters are enriched in the inner side of the actin-rich lamellipodium, they locate in the interstices of the actin meshwork. In contrast to the control cells, the WAS CTL failed to display active LFA-1 peripheral enrichment (Figure 3E). The analysis of LFA-1 distribution according to F-actin intensity confirmed the biased distribution of the LFA-1 clusters toward areas devoid of detectable F-actin in the WAS CTL (Figure 3F). Together, our data unveil the nanoscale topography of LFA-1 at the immunological synapse. They reveal that active LFA-1 distributes into hundreds of nanoclusters embedded into the actin cytoskeleton meshwork. They further identify that WASP regulates actin meshwork organization at the CTL synapse and is required to maintain the synaptic belt of active LFA-1 nanoclusters at this site.

### WASP Controls LFA-1 Organization and Activation at the Cellular and Nanometric Scales

Beyond the abnormal LFA-1 nanocluster distribution characterized in the WAS CTL by SIM, we sought to apply dSTORM to quantify whether the reduced LFA-1 activation in WAS CTL might be related to a reduced number or density of individual LFA-1 clusters. As observed earlier with TIRFM and SIM, WAS CD8<sup>+</sup> T cells were able to spread, although in a less radial manner than control T cells (Figures 4A and 4B, left panels). In particular, the typical ring of active LFA-1 clusters was disrupted in numerous WAS CTLs, and those clusters appeared to distribute more centrally (Figures 4A, 4B, S3A, and S3B). At the nanometric scale, active LFA-1 in the control CTL appeared to distribute almost exclusively into dense clusters (Figure 4A, second row of panels), in agreement with the SIM observations. This was confirmed by the density-based spatial clustering of applications with noise (DBSCAN) analysis (Ester et al., 1996) on two representative regions of interest (ROIs) within the LFA-1 ring (Figure 4A, third row of panels). In the WAS CTL, although active LFA-1 assembled into clusters, the compactness and distribution of those clusters appeared to be affected (Figure 4B, second row of panels). Indeed, the DBSCAN analysis on two representative ROIs within the preserved section of the LFA-1 ring shows that active LFA-1 clusters in the WAS CTL were less dense and less clearly delineated than those in the control CTL (Figure 4B, third row of

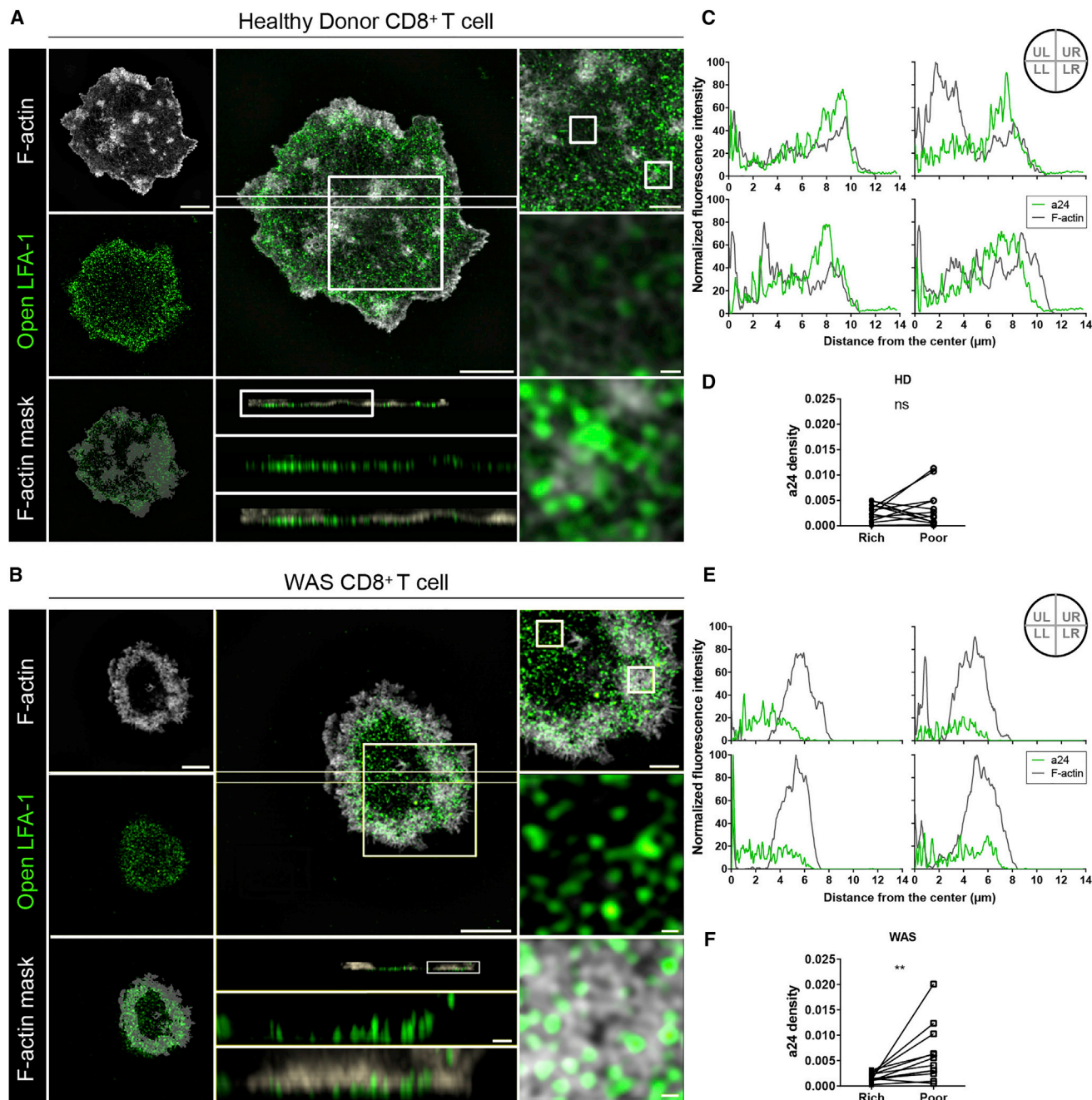


**Figure 3. Open-Conformation LFA-1 Distributes as Nanoclusters into Actin Meshwork Interstices**

(A) Basal section of SIM imaging of a representative cell from a healthy donor (HD) adhering to ICAM-1/anti-CD3 coated surface for 10 min prior to fixation. In middle panels, an overlay of the two colors (xy) is represented with orthogonal views (xz). Right panels represent different zooms. Scale bars indicate 5, 2, 1, and 0.2  $\mu\text{m}$  for whole-cell images, intermediary zoom, orthogonal views, and zoomed insets, respectively.

(B) Basal section of SIM imaging of a representative cell from a WAS patient, imaged as described in (A). Scale bars are as defined in (A).

(C) 90 $^{\circ}$ -radial profile angle of open LFA-1 and F-actin, from the center to the periphery, of the HD CTL. Intensities were normalized based on the maximum intensity.

(D) Open LFA-1 cluster density in (“rich”) or out (“poor”) of the F-actin mask for the HD CTL; n = 12 cells.

(E) 90 $^{\circ}$ -radial profile angle of open LFA-1 and F-actin, as in (C) for the WAS CTL.

(F) Open LFA-1 density in the “rich” F-actin versus “poor” F-actin area for the WAS CTL; n = 12 cells.

Statistical significances were obtained with a two-tailed Wilcoxon paired test. ns,  $p > 0.05$ ; \*\* $0.001 < p < 0.01$ . UL, upper left; UR, upper right; LL, lower left; LR, lower right.

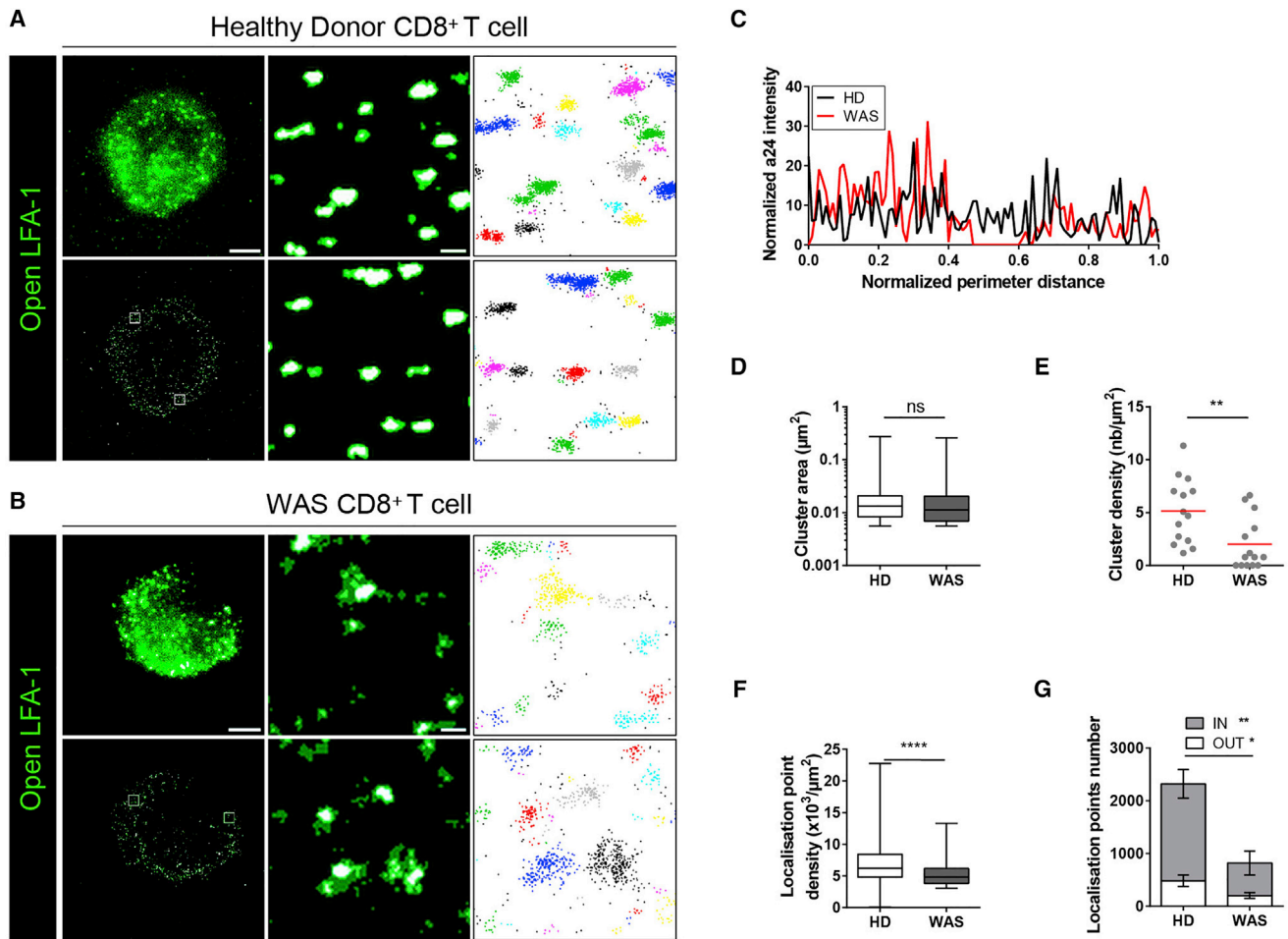


**Figure 4. LFA-1 Nanoclusters Are Relaxed and Hypodense in WASP-Deficient CD8<sup>+</sup> T Cells**

(A) Open-conformation LFA-1 staining in a representative healthy donor (HD) CTL spreading on ICAM-1/anti-CD3 Ab for 10 min prior to fixation. From left to right, TIRFM image (top) and dSTORM reconstruction (bottom), then 2 ROIs (top and bottom) with the corresponding DBSCAN detection of clusters (top and bottom). Scale bars, 5  $\mu\text{m}$  (whole cell) and 0.2  $\mu\text{m}$  (ROI).

(B) Open-conformation LFA-1 staining (a24 Ab) in a representative WAS patient CTL, treated as described in (A).

(C) Open-conformation LFA-1 intensity profile along the LFA-1 ring. Intensities and distances were normalized based on the respective maximum values for each cell.

(D) Open LFA-1 cluster area distribution within 2 ROIs per cell in control versus WAS CTLs.

(E) Surface density of open LFA-1 clusters within 2 ROIs per cell in control versus WAS CTLs. Mean is represented in red.

(F) Localization point density within 2 ROIs per cell in control versus WAS CTLs.

(G) Number of localization points detected as part of clusters (IN) or out of the clusters (OUT), within 2 ROIs per cell, in control versus WAS CTLs.  $n = 7$  cells for both HD and WAS CTLs, which were analyzed with 2 ROIs per cell.

Statistical significances were obtained with two-tailed Mann-Whitney non-parametric t tests. ns,  $p > 0.05$ ; \* $0.01 < p < 0.05$ ; \*\* $0.001 < p < 0.01$ ; \*\*\*\* $p < 0.0001$ . See also [Figure S3](#).

panels). Independently from its organization into clusters, the intensity of LFA-1 was measured along the LFA-1 ring. The WAS CTL harbored regions of poor to undetectable LFA-1 intensity (Figure 4C), highlighting the fact that it did not assemble a complete ring. To further characterize the LFA-1 activation defect associated with WASP deficiency, a number of cluster parameters were analyzed in representative ROIs of the cluster ring. Although the distribution of the areas of active LFA-1 clusters was comparable in WAS and control CTLs (Figure 4D), both the surface density of active LFA-1 cluster (Figure 4E) and their localization point density (Figure 4F) were reduced

in the WAS T cells. In addition, the proportion of localization points belonging to clusters was significantly reduced in the WAS T cells as compared to the control T cells (Figure 4G). A further analysis applied to representative cells confirmed the reduction of cluster density at the synaptic belt in WAS T cells (Figures S3C–S3E). Together, these data suggest that the reduced ability of WASP-deficient CD8<sup>+</sup> T cells to activate LFA-1 corresponds, at the cellular scale, to an incomplete assembly or stabilization of the LFA-1 ring and, at the nanometric scale, to reduced numbers of active cluster and reduced LFA-1 molecule density within those clusters.

### WASP Is Required to Confine Lytic Granules at the CTL Synapse

Given the synaptic defects of WASP-deficient cells, we reasoned that WASP might be required for the correct positioning of lytic granules. Therefore, we inspected CTLs by a 3D-SIM analysis restricted to a thickness of 550 nm from the cell surface in order to focus on the lytic granules that were the most proximal to the synaptic area. In control CTLs, lytic granules localized toward the inner layer of the high-affinity LFA-1 ring, at the edge of the actin-rich area (Figures S4A and S4B). They were detected at a close vicinity to active LFA-1 clusters in interstices of the actin cytoskeleton meshwork, suggesting that active LFA-1 clusters might control lytic granule docking at local sites of tight adhesion with the target cell. This approach was then applied to 11 control CTLs and 12 WAS CTLs. While the control CTLs adopted a synapse morphology characterized by a radial spreading, an outer ring of F-actin, and an inner ring of high-affinity LFA-1, the WAS CTLs displayed either radial synapse, distorted synapse, or elongated synapse (kinapse) morphologies (Figures 5A, S5A, and S5B). This is in agreement with our live microscopy data and previous reports on WASP-deficient CD4<sup>+</sup> T cells (Calvez et al., 2011; Lafouresse et al., 2012; Sims et al., 2007). The compilation of the control cells (Experimental Procedures) yielded a very clear topological picture composed by a thick peripheral ring of actin meshwork, followed by a partially overlapping belt of active LFA-1 clusters and by lytic granules dispersed within the confinement of the LFA-1 cluster belt (Figure 5B). Taking into account the morphological heterogeneity of the WAS CTL, images were compiled separately, according to the 3 identified morphological categories (Figure 5A). WAS CTLs forming synapses displayed a radial polarity similar to that observed in control cells, with correct confinement of the lytic granules within the LFA-1 cluster belt (Figure 5B). Differently, the cells with distorted synapses failed to reveal a clear radial organization, and the lytic granules localized over the contact planes without any apparent localization bias. The cells forming a kinapse revealed a clear longitudinal polarization, with a wide actin-rich edge, a central LFA-1-rich area, and dispersed lytic granules. To assess the lytic granule confinement function of the active LFA-1 cluster belt, the positions of individual perforin dots were overlaid on the LFA-1 mask, and their distances from the edge of the LFA-1 masks were calculated (Figures 5C and 5D). In the cells assembling a radial LFA-1 cluster belt, most detected perforin dots were positioned on the LFA-1 cluster belt, at a mean distance of 3  $\mu\text{m}$  from the outer edge of this belt (Figure 5D). In WASP-deficient T cells adopting distorted synapse or kinapse morphologies, an increased proportion of perforin dots were positioned away from the LFA-1 belt (Figure 5C) or very close to its outer edge (Figure 5D). The comparison of the WAS-related morphologies is suggestive of an interplay between actin cytoskeleton organization, LFA-1 cluster distribution, and lytic granule polarization. We next aimed to examine, by 3D-SIM, the assembly of the LFA-1 cluster belt and lytic granule positioning using anti-CD3 monoclonal Ab (mAb)-coated P815 cells. The control CTL forming a synapse with target cells displayed a flattened contact area enriched in F-actin (Figure 5E). The en-face view is in line with our observations on stimulatory surfaces. It shows a ring of active LFA-1 lying inward from the F-actin-rich area and the docking of lytic granules within the inner confines of the high-affinity

LFA-1 ring. Although the WAS CTL formed conjugates with the anti-CD3 mAb-coated P815 cells, their morphology displayed notable aberrations (Figure 5E), including the presence of lateral F-actin-rich protrusions and a non-symmetrical morphology. In the selected cell, active LFA-1 clusters were reduced in numbers and failed to form a ring. The few lytic granules detected in the synapse plane displayed a very peripheral distribution. Together, these observations confirm the role of WASP in assembling the high-affinity LFA-1 cluster belt at the CTL synapse. The WASP-deficiency model also suggests that the LFA-1 cluster belt may control the confined delivery of lytic granules.

### Relationship between LFA-1 Activation Level and Cytotoxic Activity

To further explore the possible link between LFA1 activation, nanocluster belt organization, and cytotoxic activity independently from WASP, we sought to lower LFA-1 activation in normal cells by diluting the concentration of anti-CD3 mAb, which is expected to reduce the strength of the inside-out signaling (Mueller et al., 2004). Indeed, the use of different doses of 0.1 to 10  $\mu\text{g}/\text{mL}$  anti-CD3 mAb to coat target cells resulted in a gradual activation of LFA-1 on the surface of the CTL (Figure 6A). In particular, the concentration of 1  $\mu\text{g}/\text{mL}$  anti-CD3 mAb was found to lead to an intermediate level of LFA-1 activation comparable to that reached by WAS T cells stimulated with the 10  $\mu\text{g}/\text{mL}$  anti-CD3 mAb concentration. Sub-optimal activation of LFA-1 in the control CTL was associated with a reduction in their killing activity (Figure 6B). At the nanometric scale, active LFA-1 in the control CTL stimulated with 1  $\mu\text{g}/\text{mL}$  anti-CD3 mAb distributed into dense and well-delineated clusters, as shown by the DBSCAN analysis on two representative ROIs within the LFA-1 ring (Figure S6A). The main parameter that distinguished LFA-1 nanoclusters upon stimulation with the 1- $\mu\text{g}/\text{mL}$  and 10- $\mu\text{g}/\text{mL}$  anti-CD3 mAb concentrations was their surface (Figures 4E and S6B), indicating that suboptimal LFA-1 activation corresponds to the assembly of smaller clusters and suggesting a concentration-dependent increase of active LFA-1 cluster size. Of note, active LFA-1 nanoclusters distributed into a belt-like structure, independently from the anti-CD3 mAb concentrations used. We next investigated, using video-microscopy, the mechanism by which suboptimal activation of LFA-1 in normal CTLs might be related to the reduced killing activity (Figure 6C). At the high anti-CD3 mAb concentration, most CTLs entering in contact with a target cell were able to kill it over the 150-min observation time (Figure 6D). While the lethal hit delivery was rapid (<20 min), CTLs remained attached to the dying target cells for a prolonged time (approximately 50 min), as previously reported (Wiedemann et al., 2006). Differently, at the intermediate anti-CD3 Ab concentration, about one third of the CTLs entering in contact with a target cell failed to kill it over the observation time, which matches the reduced killing activity observed. Interestingly, ineffective and productive CTLs diverged in their attachment stability, as revealed by the interaction time with the target cells (respectively, 20 and 50 min). This analysis, therefore, shows that lowering TCR triggering in normal cells reduces LFA-1 activation and is associated with an increased proportion of cells that display reduced ability to form stable contacts with target cells.



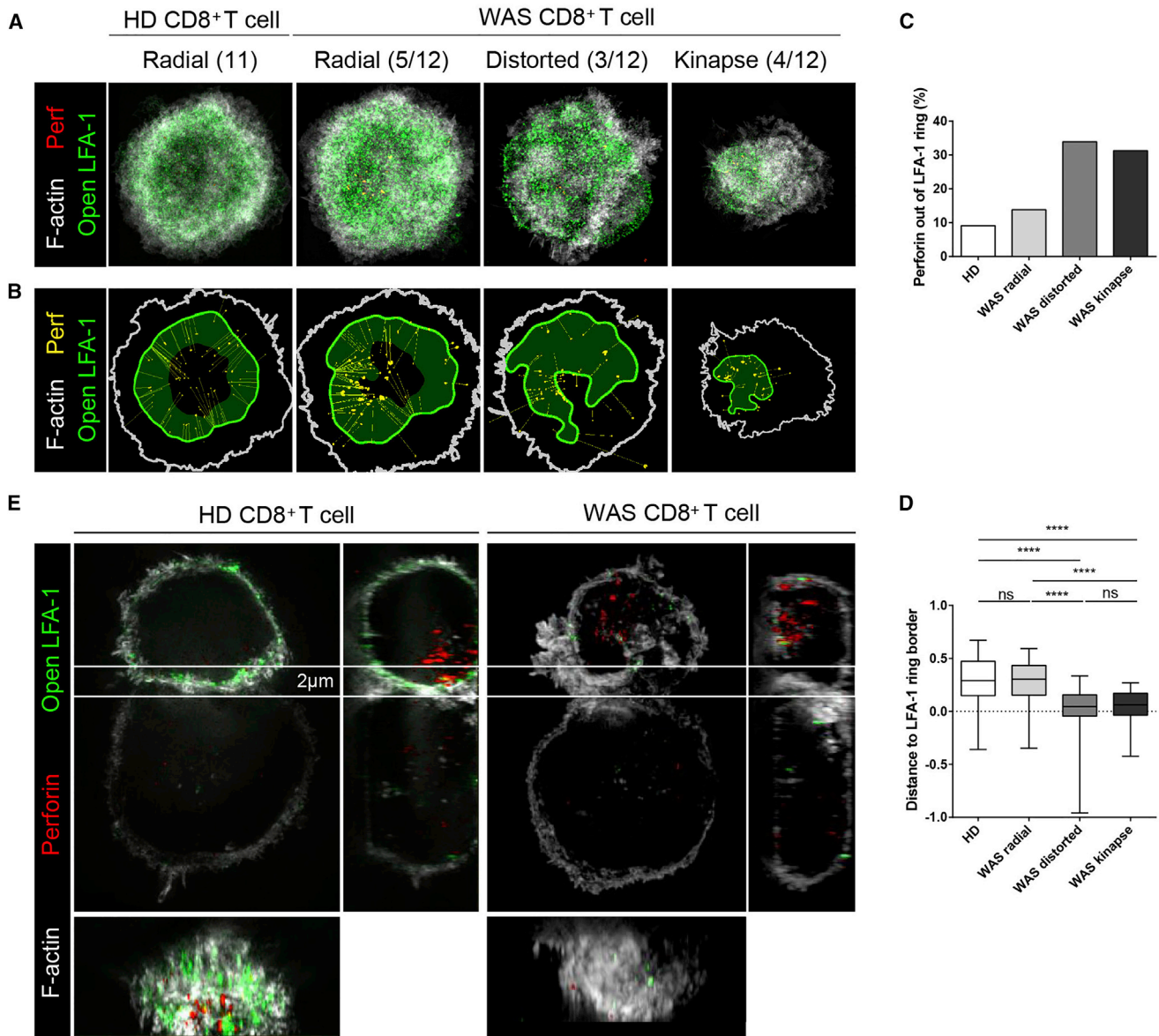


**Figure 5. Defects of LFA-1 Cluster Belt Assembly and Lytic Granule Positioning in WASP-Deficient CD8<sup>+</sup> T Cells**

(A) Compilation of SIM images of HD and WAS CTLs spreading on ICAM-1/anti-CD3 Ab for 10 min prior to fixation. WAS CTLs were split into “radial,” “distorted,” and “kinapse” categories, according to morphological parameters.

(B) Open LFA-1 mask corresponding to images shown in (A), overlaid with a distance map of individual perforin dots to the outer border of LFA-1 mask and the outline of the F-actin.

(C) Percentage of perforin dots detected outside of LFA-1 mask outer border.

(D) Distance of all perforin dots to LFA-1 mask outer border reported to the radius distance of the corresponding compiled cell.

(E) SIM imaging of a representative control and a WAS CTL in contact with a target cell pre-coated with anti-CD3 Ab. Bottom panels represent the synaptic area in contact with the target cell.

Statistical significances were obtained with a two-tailed Mann-Whitney non-parametric t test. ns,  $p > 0.05$ ; \*\*\*\* $p < 0.0001$ .

See also [Figures S4](#) and [S5](#).

## DISCUSSION

In this study, we set out to explore the precise topography of LFA-1 at the immunological synapse of WAS patient-derived CD8<sup>+</sup> T cells. A combination of advanced microscopy modalities allowed us not only to identify a defect in LFA-1 activation

but also to produce fundamental knowledge about the interplay between actin cytoskeleton meshwork organization, LFA-1 activation, and lytic granule docking.

Since the initial description of the immunological synapse, the distribution of LFA-1 as a peripheral ring has been a hallmark of this structure ([Grakoui et al., 1999](#); [Monks et al.,](#)

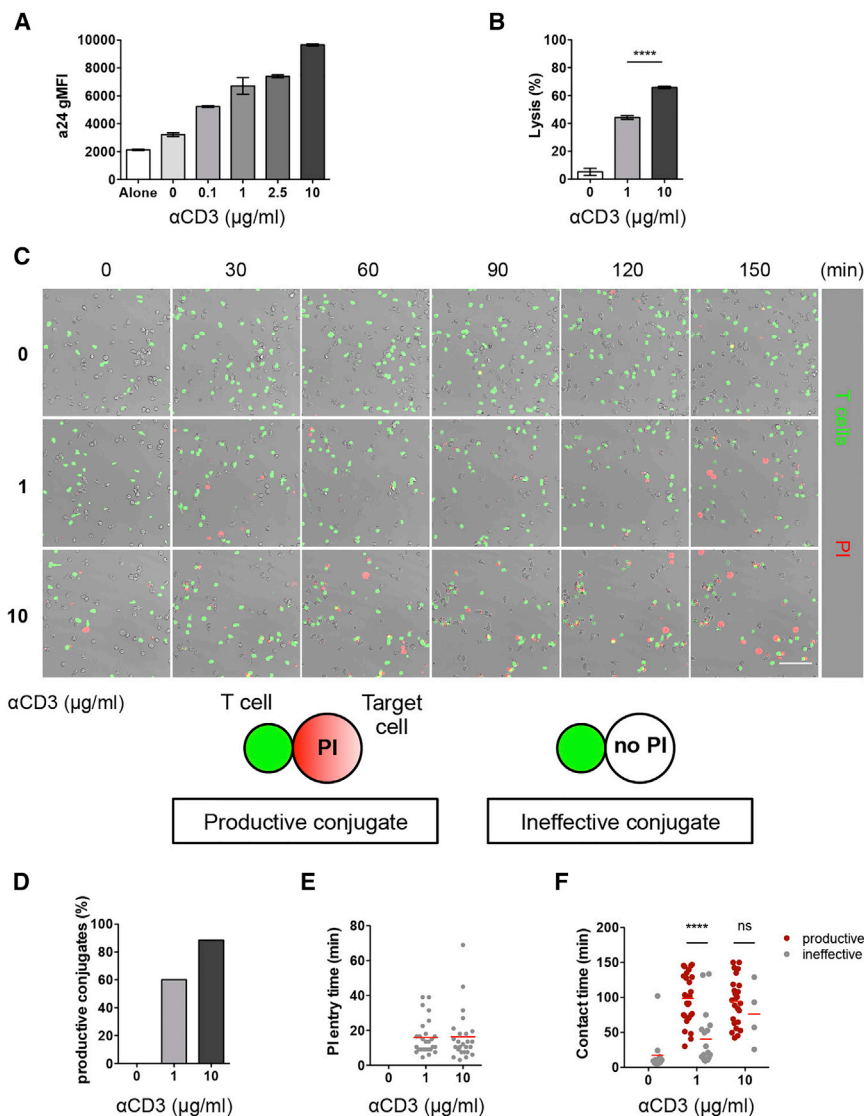


**Figure 6. Sub-optimal TCR Stimulation of Normal CTL Leads to Reduced LFA-1 Activation and Killing Efficiency**

(A) LFA-1 activation measured by flow cytometry with the a24 Ab after 30-min interaction of HD cells with P815 cells pre-coated with the indicated anti-CD3 mAb concentrations.  $n = 3$  experiments.

(B) Number of residual alive target cells after 4 hr of a redirected killing assay at a 2:1 E:T ratio against P815 cells pre-coated with 1 or 10  $\mu$ g/mL anti-CD3 mAb.

(C) Target cells (coated with 0, 1, or 10  $\mu$ g/mL anti-CD3 mAb) were seeded in the presence of HD CTL (green) at a 2:1 E:T ratio. PI (red) was used to track lethal hit delivery. Scale bar, 100  $\mu$ m.

(D) Proportion of productive CTL to target cell conjugates, based on the detection of PI within the observation time window of 150 min.

(E) Within productive conjugates, time delay between initial CTL to target cell contact and PI entry.

(F) Contact time between CTL and target cells, distinguishing productive conjugates from ineffective conjugates.

Error bars indicate mean  $\pm$  SEM. Statistical significances were obtained with two-tailed Mann-Whitney non-parametric t test. ns,  $p > 0.05$ ; \*\*\*\* $p < 0.0001$ .

See also Figure S6.

1998). It is, however, only recently that the conformational state of LFA-1 at the immunological synapse has been unraveled with the use of conformation-specific antibodies (Comrie et al., 2015). Still, the precise topography of LFA-1 remained to be established. In agreement with a previous report in Jurkat cells (Kaizuka et al., 2007), we observed by TIRFM that, upon synapse assembly, primary human CD8<sup>+</sup> T cells appear to aggregate LFA-1 into microdomains. However, the 2 super-resolution microscopy approaches used in our study highlight that the structures appearing as microdomains correspond to areas densely populated by well-individualized nanoclusters. The diameter of the LFA-1 clusters detected here in T lymphocytes is approximately 100 nm, which is comparable to that measured by transmission electron microscopy (TEM) at the surface of monocytes (Cambi et al., 2006). We report that LFA-1 clusters in the open conformation were concentrated into a belt-like structure, in line with the

LFA-1 ring described previously (Comrie et al., 2015; Kaizuka et al., 2007). High-affinity LFA-1 molecules are expected to bind tightly the actin cytoskeleton (Cairo et al., 2006) to permit a tensile force-driven activation mechanism (Nordenfelt et al., 2016). In line with such a central role of the actin cytoskeleton in the control of LFA-1 activation and distribution, our radial analysis of LFA-1 and F-actin intensities showed that the open LFA-1 clusters lay in the inner layer of peripheral actin ring. More unexpectedly however, our 2D analysis revealed that the LFA-1 clusters were positioned into the interstices of the actin cytoskeleton meshwork. Our 3D imaging approach further revealed that the innermost sections of the LFA-1 clusters stood on a deeper layer of the actin cytoskeleton. Our analysis, therefore, posits the question of how LFA-1 clusters are coupled to the actin cytoskeleton. We favor the hypothesis that the most superficial layer of the actin cytoskeleton might provide a physical meshwork to laterally constrain LFA-1 nanoclusters, while the underlying layer might provide a site for physical coupling and force transmission via Talin-1 and Kindlin-3 (Evans et al., 2009).

In accordance with this hypothesis, deficiency of the actin regulator WASP was found to affect the molecular density of individual active clusters as well as their number. Interestingly, WASP is also involved in the assembly of F-actin foci beneath TCR microclusters to facilitate PLC $\gamma$ 1 activation and calcium flux (Kumari et al., 2015). This suggests that distinct F-actin

microarchitectures are associated with TCR and LFA-1 nanoclusters to sustain their specific activation patterns. Indeed, the use of micropatterns has revealed different actin cytoskeleton dynamics associated with the TCR and LFA-1 (Tabdanov et al., 2015). Importantly, here, we identified WASP as a key protein to control the assembly of the circular belt of high-affinity LFA-1 clusters at the CTL synapse, which allowed us to investigate the role of this structure in controlling the cytotoxic activity. Our data indicate that, while WASP appears to regulate the confinement and activation of LFA-1 clusters at the nanometric scale, it also controls their distribution at the cellular scale. It is probable that defective confinement of the LFA-1 nanoclusters leads to the different distribution patterns observed in the WAS CTL. Given the role of WASP in transducing TCR signals (Kumari et al., 2015), the LFA-1 defects associated with WASP deficiency reported here might originate from a lower TCR-evoked activation. We found that stimulation of normal CTLs with an intermediate anti-CD3 mAb concentration led to reduced LFA-1 activation and killing efficiency. However, we failed to detect cells with a disrupted LFA-1 cluster belt and with central localization of clusters, as observed in numerous WAS CTLs. At the nanometric scale, control CTLs stimulated with 1  $\mu$ g/mL anti-CD3 Ab assembled smaller LFA-1 clusters, in which compactness was, however, not affected as in the case of the WASP-deficient CTLs. Together, these observations indicate that the WAS-related defect cannot be simply explained by a reduced LFA-1 activation. The perturbed morphology of the WAS CTL revealed here might result in a broad perturbation of the distribution of membrane receptor beyond LFA-1. However, WASP deficiency does not appear to affect TCR microcluster distribution and dynamics (Kumari et al., 2015) or the exclusion of CD45 from the synapse area (Calvez et al., 2011). Together, these observations suggest that WASP-controlled actin remodeling is particularly important for the control of LFA-1 distribution and activation.

Cytotoxic T cells assemble a LFA-1/talin ring junction through which lytic granules are secreted (Somersalo et al., 2004; Stinchcombe et al., 2001). Lytic granules have been shown to release their contents by fusing with an actin-depleted secretory domain located toward the synapse center (Ritter et al., 2015; Stinchcombe et al., 2001; Stinchcombe et al., 2006). An alternative model of lytic granule secretion has recently been proposed based on the observation that lytic granule secretion, visualized with a fluorescent probe, occurred in an intermediate domain of the synapse corresponding to the inner side of the F-actin ring (Basu et al., 2016). Interestingly, measurement of local mechanical forces with micropillars revealed that this domain is where the strongest forces are exerted. This model implies that lytic granules are secreted in synaptic areas containing the adhesive and cytoskeletal machinery required to transmit force. In support of this model, our experiments with healthy donor CTLs indicate that lytic granules would preferentially dock at the vicinity of high-affinity LFA-1 clusters in the inner side of the LFA-1 cluster belt associated to a relatively dense actin meshwork. In conjunction with this mechanism, local actin meshwork relaxation might be required for lytic granule exocytosis as described in natural killer (NK) cells (Brown et al., 2011; Rak et al., 2011). Taken together, these observations suggest that lytic granules would

be preferentially secreted in the inner side of the LFA-1 cluster belt, providing optimal local forces to control both secretion and target cell interaction. We argue that the reduced lytic activity of WAS CTLs is, at least in part, related to a reduced LFA-1 activation and symmetry. Indeed, we previously reported that both conjugate formation and LAMP-1 exposure are not affected by WASP deficiency (Calvez et al., 2011; De Meester et al., 2010). Similarly, the reduction of CTL cytolytic activity induced by LFA-1 with Fab fragments was not associated with granule release inhibition but with non-polarized delivery (Anikeeva et al., 2005). In a physiological setting, the ability to dissolve and reform the adhesion ring would be required for CTLs to execute multiple killing. Accordingly, our data point to an amplification of the WASP-associated killing defect in long-term assays, in which multiple killing is favored (Vasconcelos et al., 2015). Beyond the WASP-deficiency model, our study indicates that the level of LFA-1 activation might regulate killing efficiency. Indeed, stimulation of CTLs with an intermediate anti-CD3 mAb concentration leading to reduced LFA-1 activation is associated with a lower killing activity. This is explained by the increased frequency of individual CTLs, which establish poorly stable contacts with target cells and fail to kill. Together, our data on the WASP-deficiency CTL model and the suboptimal activation of normal CTLs suggest that both quantitative and qualitative aspects of LFA-1 activation at the nanoscale contribute to the tuning of killing efficacy.

In conclusion, our study provides a detailed characterization of LFA-1 topography at the human T cell synapse. It provides insight into the activation of LFA-1 at the nanoscale and into its interaction with the underlying actin cytoskeleton meshwork. It further identifies WASP as a key protein to control the LFA-1 cluster belt that confines lytic granule secretion.

## EXPERIMENTAL PROCEDURES

### Patients and Cells

Blood samples from WAS patients and healthy donors were obtained following standard ethical procedures (Helsinki protocol) and as per French Bioethics law and with the approval of the local ethics committee. Peripheral blood mononuclear cells (PBMCs) were isolated by density gradient centrifugation over a Ficoll gradient (PAA Laboratories). CD8<sup>+</sup> T cells were isolated by negative selection according to the manufacturer's instructions (STEMCELL Technologies). T cells were cultured in RPMI 1640 GlutaMAX (GIBCO) supplemented with 5% human serum (PAA) and stimulated every 2 weeks with irradiated PBMCs and Epstein-Barr virus (EBV)-transformed JY cells in the presence of 1  $\mu$ g/mL phyto-hemagglutinin (PHA), 100 IU/mL recombinant human interleukin (rhIL)-2, and 5 ng/mL rhIL-15. WAS CTLs were derived from the patient W2 described previously (Trifari et al., 2006), as well as from patients WAS1 (De Meester et al., 2010) and WAS4 (Marangoni et al., 2007). The lack of WASP expression in the patient-derived CD8<sup>+</sup> T cells was confirmed by western blotting as previously reported (Trifari et al., 2006). GFP-expressing P815 cells were generated by lentiviral transduction and cultured in DMEM (GIBCO) supplemented with 10% FCS (PAA).

### Flow Cytometry

CTLs were stained with anti-CD8-FITC (fluorescein isothiocyanate) mAb and anti-CD4-PE mAb for 20 min at 4°C, fixed with 3% paraformaldehyde (PFA), and permeabilized with PBS 3% BSA 0.1% saponin. Intracellular staining with anti-WASP 5A5 mAb was followed by phycoerythrin (PE)-labeled secondary Ab. Granzyme B and perforin staining were performed with FITC-labeled mAb and AF647-labeled mAb (dG9). LFA-1 expression was

revealed with mAb for total (TS2/4) or open conformations (a24). To measure LFA-1 activation, CTLs were incubated with GFP-expressing target cells previously coated with anti-CD3 mAb (OKT3, eBioscience). Unlabeled a24 mAb was added at 2.5  $\mu\text{g}/\text{mL}$  during a 1-hr incubation at 37°C. Cells were fixed with 3% PFA, and the bound a24 mAb was revealed with AF647-labeled secondary Ab. Antibodies were purchased from BD Pharmingen. Data were acquired on the BD FACSCalibur cytometer and analyzed with FlowJo software.

### Cytotoxic Assays

For the flow-cytometry-based assessment of CTL cytotoxic activity, GFP-expressing P815 target cells and CTLs were prepared as described for LFA-1 activation. Cells were pelleted for 1 min at 1,500 rpm and incubated at 37°C/5%  $\text{CO}_2$  from 4 to 24 hr. Aphidicolin (Sigma) was used at 0.1  $\mu\text{g}/\text{mL}$  during the duration of the assay to block target cell proliferation. Residual alive target cell acquisition and quantification were performed as described previously (Vasconcelos et al., 2015). All data were acquired on a BD FACSCalibur cytometer and analyzed using FlowJo software. For the microscopy-based assessment of CTL cytotoxic activity, 8-well IBIDI chambers were coated with 10  $\mu\text{g}/\text{mL}$  of fibronectin (Sigma-Aldrich) for 1 hr at 37°C/5%  $\text{CO}_2$ . CTLs were pre-stained with CellTracker Green CMFDA dye (Invitrogen) for 30 min at 37°C/5%  $\text{CO}_2$  and then transferred to an IBIDI chamber together with P815 cells pre-coated with anti-CD3 mAb as described for LFA-1 activation. A 200- $\mu\text{M}$  concentration of propidium iodide (PI) was added in the medium and present during the acquisition on a Leica SP8 confocal microscope equipped with a chamber set at 37°C/5%  $\text{CO}_2$ .

### TIRFM

8-well Labteck chamber slides with a #1.5-glass bottom were coated overnight with both recombinant ICAM-1/Fc chimera (4  $\mu\text{g}/\text{mL}$ ) (R&D Systems, Minneapolis, MN, USA) and anti-CD3 mAb (10  $\mu\text{g}/\text{mL}$ ) at 4°C. Cells were stained with 2  $\mu\text{M}$  SiR-actin for 1 hr at 37°C before transferring onto the Labteck chamber slides. Acquisitions were performed by TIRFM illumination integrated within an iLas2 system (Roper Scientific, Lisses, France) incorporated within an inverted motorized microscope (Nikon Ti, Japan) equipped with a Plan-Apo 100 $\times$  1.45 NA objective and a perfect focus system. Live samples were imaged at 37°C with 5%  $\text{CO}_2$ . Images were acquired at 1.26–1.29 s per frame for 10 min using MetaMorph software (Molecular Devices, Sunnyvale, CA, USA). The emitted photons were collected with a 512  $\times$  512 EM-CCD (electron multiplying charge-coupled device) camera (Evolve; Photometrics, Tucson, AZ, USA).

### dSTORM

#1.5H circular coverslips were coated overnight with recombinant ICAM-1/Fc chimera and anti-CD3 mAb at 4°C. AF647-labeled a24 mAb was added to CTLs during their attachment to the coverslips. After 10 min at 37°C, cells were fixed with 4% PFA. Acquisition was performed by TIRFM illumination on the system described earlier. Images were acquired at room temperature (RT) in a solution containing Cysteamine (Sigma, USA) and glucose oxidase (Sigma, USA) as oxygen scavenger. The AF647 fluorescence was converted into a dark state using a 640-nm laser. Upon obtaining the adequate density of blinking events per frame, 20,000 frames were acquired at 50–100 Hz. Images were reconstructed online using the WaveTracer module (Kechkar et al., 2013) integrated into MetaMorph (20-nm pixel size). The minimal surface of a LFA-1 cluster was set as twice the mean surface of the events detected outside the cells, resulting in a value of 0.0055  $\mu\text{m}^2$ . On that basis, we used the DBSCAN algorithm to identify clusters in zoomed insets measuring 1.6  $\mu\text{m}$   $\times$  1.6  $\mu\text{m}$ . The cluster detection was set as a minimum of 3 points within a radius of 20–40 nm (epsilon). Shape and area were extracted with ggplot2 and factoextra in R software. We wrote a C++ algorithm to determine the size of clusters in nanometers. Whole-cell cluster counts were measured using ImageJ with an intensity-based threshold. The ImageJ particle detection approach was validated by comparison to DBSCAN in test ROIs.

### SIM

The staining procedure was comparable to that used for dSTORM with the following combination: AF568-labeled a24 mAb, phalloidin-AF647, and,

where indicated, anti-perforin mAb revealed with an AF488-labeled secondary Ab. For conjugates, CTL and P815 cells were seeded in U-bottom 96-well plates with AF-568-labeled a24 mAb and then were transferred onto poly-L-lysine-coated #1.5H coverslips for 10 min at 37°C. Fixation and permeabilization were executed as described earlier, and F-actin and perforin were stained by phalloidin-AF488- and AF647-labeled anti-perforin mAbs for 1 hr at RT. Coverslips were mounted in Vectashield H-1000 (Vector Laboratories, Burlingame, CA, USA). 3D-SIM images were acquired with a Zeiss ELYRA PS1 super resolution (SR)-SIM equipped with a Plan-Apo 63 $\times$ /1.40 NA oil DIC (differential interference contrast) immersion objective using a scientific complementary metal-oxide-semiconductor (sCMOS) camera (Hamamatsu) and a 1.60 $\times$  tube lens. A multicolor image was obtained with the 488-nm, 561-nm, and 642-nm laser excitations using the 28- $\mu\text{m}$ , 32- $\mu\text{m}$ , and 42- $\mu\text{m}$  optical grids, respectively, which were rotated to three pre-aligned angles and translated to 5 positions per angle. The different channels were aligned using the point spread function (PSF) from multicolor beads. The lateral pixel size was 65 nm in the acquired images and 32 nm in the reconstructed images. The 3D-SIM images were reconstructed with the Zeiss ZEN software and further verified with SIMcheck (suite of ImageJ plugins). 3D-SIM images of 550-nm thickness were analyzed by ImageJ. Thresholds were performed on F-actin and a24 intensity to transform them into two masks; then, the number of a24 clusters in and out of the F-actin mask were extracted and reported to the surface area of the mask. Individual cells were normalized according to each cell area before compilation. LFA-1 ring mask was determined by a Gaussian blur and an intensity threshold. The closest distance of each perforin granule to the outer border of the ring was drawn manually and reported to the radius of the compiled cell.

### Statistical Analysis

Statistical analyses were performed using GraphPad software. Statistical significance was determined by performing two-tailed non-parametric paired Mann-Whitney or unpaired Wilcoxon *t* tests. Graphs indicate mean values  $\pm$  SEM. Resulting *p* values are indicated as follows: ns, *p* > 0.05; \*0.01 < *p* < 0.05; \*\*0.001 < *p* < 0.01; \*\*\**p* < 0.001; and \*\*\*\**p* < 0.0001.

### SUPPLEMENTAL INFORMATION

Supplemental information includes six figures and two movies and can be found with this article online at <https://doi.org/10.1016/j.celrep.2017.12.088>.

### ACKNOWLEDGMENTS

We wish to thank Astrid Canivet and Daniele Daviaud from the CPTP microscopy platform, as well as Fatima-Ezzahra L'Faqihi-Olive, Valérie Duplan-Eche, and Anne-Laure Iscache from the CPTP cytometry platform. We are grateful for the support and advice of Frédérique Gaits-Iacovoni and Madjid Zanoun from the Cellular Imaging Facility Ranguelil-I2MC/TRI platform. We wish to thank Nancy Hogg for generously providing the a24 antibody. We are grateful to Johannes Huppa, René Platzer, Jean-Baptiste Sibarita, Kaan Boztug, Sabina Müller, Liza Filali, Laurène Pfajfer, Yolla German, Marie-Pierre Puissegur, Fanny Lafouresse, and Rana Mansour for technical advice and discussion. This work was supported by the Brazilian post-doctoral programs from CAPES (6486/10-0) and CNPq (237654/2012-1). This work also benefited from funding from the Fondation ARC pour la Recherche sur le Cancer (grant EML2012090493), the Institut National Du Cancer (grant INCa 2012-054), the CNRS (Mission pour l'Interdisciplinarité, AAP Inter-Instituts), the Agence Nationale de la Recherche (Laboratoire d'Excellence Toulouse Cancer), the Région Occitanie (grant RBIO 2015), and the Fondation Toulouse Cancer Santé. D.G. is recipient of a Cifre convention between the French National Association of Technological Research and TxCell (2014/0916). The funders had no role in study design, data collection and analysis, decision to publish, or preparation of the manuscript.

### AUTHOR CONTRIBUTIONS

R.H. performed the super-resolution microscopy experiments, analyzed the results, and contributed to the manuscript preparation. D.G. performed the

functional assays, analyzed the results, and contributed to the manuscript preparation. J.R.-B. performed data analysis. Z.V. performed the initial characterization of LFA-1 activation at the CTL synapse. J.C. and M.M. contributed to data analysis. N.D. contributed to data analysis and to manuscript editing. S.V. discussed data and ideas and edited the manuscript. S.A. contributed to the design of the study, supervised super-resolution microscopy experiments, analyzed data, and contributed to the manuscript preparation. L.D. designed the research, supervised the experimental and analytical work, and wrote the paper.

## DECLARATION OF INTERESTS

The authors declare no competing interests.

Received: May 29, 2017

Revised: November 1, 2017

Accepted: December 22, 2017

Published: January 23, 2018

## REFERENCES

- Anikeeva, N., Somersalo, K., Sims, T.N., Thomas, V.K., Dustin, M.L., and Sykulev, Y. (2005). Distinct role of lymphocyte function-associated antigen-1 in mediating effective cytolytic activity by cytotoxic T lymphocytes. *Proc. Natl. Acad. Sci. USA* *102*, 6437–6442.
- Basu, R., Whitlock, B.M., Husson, J., Le Floch, A., Jin, W., Oylar-Yaniv, A., Dotiwala, F., Giannone, G., Hivroz, C., Biais, N., et al. (2016). Cytotoxic T cells use mechanical force to potentiate target cell killing. *Cell* *165*, 100–110.
- Baumgart, F., Arnold, A.M., Leskova, K., Staszek, K., Fölser, M., Weghuber, J., Stockinger, H., and Schütz, G.J. (2016). Varying label density allows artifact-free analysis of membrane-protein nanoclusters. *Nat. Methods* *13*, 661–664.
- Brown, A.C., Oddos, S., Dobbie, I.M., Alakoskela, J.M., Parton, R.M., Eissmann, P., Neil, M.A., Dunsby, C., French, P.M., Davis, I., and Davis, D.M. (2011). Remodelling of cortical actin where lytic granules dock at natural killer cell immune synapses revealed by super-resolution microscopy. *PLoS Biol.* *9*, e1001152.
- Cairo, C.W., Mirchev, R., and Golan, D.E. (2006). Cytoskeletal regulation couples LFA-1 conformational changes to receptor lateral mobility and clustering. *Immunity* *25*, 297–308.
- Calvez, R., Lafouresse, F., De Meester, J., Galy, A., Valitutti, S., and Dupré, L. (2011). The Wiskott-Aldrich syndrome protein permits assembly of a focused immunological synapse enabling sustained T-cell receptor signaling. *Haematologica* *96*, 1415–1423.
- Cambi, A., Joosten, B., Koopman, M., de Lange, F., Beeren, I., Torensma, R., Fransen, J.A., Garcia-Parajó, M., van Leeuwen, F.N., and Figdor, C.G. (2006). Organization of the integrin LFA-1 in nanoclusters regulates its activity. *Mol. Biol. Cell* *17*, 4270–4281.
- Comrie, W.A., Babich, A., and Burkhardt, J.K. (2015). F-actin flow drives affinity maturation and spatial organization of LFA-1 at the immunological synapse. *J. Cell Biol.* *208*, 475–491.
- Davignon, D., Martz, E., Reynolds, T., Kürzinger, K., and Springer, T.A. (1981). Lymphocyte function-associated antigen 1 (LFA-1): a surface antigen distinct from Lyt-2,3 that participates in T lymphocyte-mediated killing. *Proc. Natl. Acad. Sci. USA* *78*, 4535–4539.
- De Meester, J., Calvez, R., Valitutti, S., and Dupré, L. (2010). The Wiskott-Aldrich syndrome protein regulates CTL cytotoxicity and is required for efficient killing of B cell lymphoma targets. *J. Leukoc. Biol.* *88*, 1031–1040.
- Dupré, L., Aiuti, A., Trifari, S., Martino, S., Saracco, P., Bordignon, C., and Roncarolo, M.-G. (2002). Wiskott-Aldrich syndrome protein regulates lipid raft dynamics during immunological synapse formation. *Immunity* *17*, 157–166.
- Ester, M., Kriegel, H.-P., Sander, J., and Xu, X. (1996). A density-based algorithm for discovering clusters in large spatial databases with noise. In *Proceedings of the Second International Conference on Knowledge, Discovery and Data Mining*, E. Simoudis, J. Han, and U. Fayyad, eds. (AAAI Press), pp. 226–231.
- Evans, R., Patzak, I., Svensson, L., De Filippo, K., Jones, K., McDowall, A., and Hogg, N. (2009). Integrins in immunity. *J. Cell Sci.* *122*, 215–225.
- Grakoui, A., Bromley, S.K., Sumen, C., Davis, M.M., Shaw, A.S., Allen, P.M., and Dustin, M.L. (1999). The immunological synapse: a molecular machine controlling T cell activation. *Science* *285*, 221–227.
- Gustafsson, M.G. (2000). Surpassing the lateral resolution limit by a factor of two using structured illumination microscopy. *J. Microsc.* *198*, 82–87.
- Heilemann, M., van de Linde, S., Schüttelpe, M., Kasper, R., Seefeldt, B., Mukherjee, A., Tinnefeld, P., and Sauer, M. (2008). Subdiffraction-resolution fluorescence imaging with conventional fluorescent probes. *Angew. Chem. Int. Ed. Engl.* *47*, 6172–6176.
- Kaizuka, Y., Douglass, A.D., Varma, R., Dustin, M.L., and Vale, R.D. (2007). Mechanisms for segregating T cell receptor and adhesion molecules during immunological synapse formation in Jurkat T cells. *Proc. Natl. Acad. Sci. USA* *104*, 20296–20301.
- Kechkar, A., Nair, D., Heilemann, M., Choquet, D., and Sibarita, J.B. (2013). Real-time analysis and visualization for single-molecule based super-resolution microscopy. *PLoS ONE* *8*, e62918.
- Kumari, S., Depoil, D., Martinelli, R., Judokusumo, E., Carmona, G., Gertler, F.B., Kam, L.C., Carman, C.V., Burkhardt, J.K., Irvine, D.J., and Dustin, M.L. (2015). Actin foci facilitate activation of the phospholipase C- $\gamma$  in primary T lymphocytes via the WASP pathway. *eLife* *4*, e04953.
- Lafouresse, F., Cotta-de-Almeida, V., Malet-Engra, G., Galy, A., Valitutti, S., and Dupré, L. (2012). Wiskott-Aldrich syndrome protein controls antigen-presenting cell-driven CD4+ T-cell motility by regulating adhesion to intercellular adhesion molecule-1. *Immunology* *137*, 183–196.
- Lang, P.A., Shaabani, N., Borkens, S., Honke, N., Scheu, S., Booth, S., Brenner, D., Meryk, A., Barthuber, C., Recher, M., et al. (2013). Reduced type I interferon production by dendritic cells and weakened antiviral immunity in patients with Wiskott-Aldrich syndrome protein deficiency. *J. Allergy Clin. Immunol.* *131*, 815–824.
- Lukinavicius, G., Reymond, L., D'Este, E., Masharina, A., Göttfert, F., Ta, H., Güther, A., Fournier, M., Rizzo, S., Waldmann, H., et al. (2014). Fluorogenic probes for live-cell imaging of the cytoskeleton. *Nat. Methods* *11*, 731–733.
- Marangoni, F., Trifari, S., Scaramuzza, S., Panaroni, C., Martino, S., Notarangelo, L.D., Baz, Z., Metin, A., Cattaneo, F., Villa, A., et al. (2007). WASP regulates suppressor activity of human and murine CD4(+)CD25(+) FOXP3(+) natural regulatory T cells. *J. Exp. Med.* *204*, 369–380.
- Monks, C.R., Freiberg, B.A., Kupfer, H., Sciaky, N., and Kupfer, A. (1998). Three-dimensional segregation of supramolecular activation clusters in T cells. *Nature* *395*, 82–86.
- Mueller, K.L., Daniels, M.A., Felthouser, A., Kao, C., Jameson, S.C., and Shimizu, Y. (2004). Cutting edge: LFA-1 integrin-dependent T cell adhesion is regulated by both ag specificity and sensitivity. *J. Immunol.* *173*, 2222–2226.
- Murugesan, S., Hong, J., Yi, J., Li, D., Beach, J.R., Shao, L., Meinhardt, J., Madison, G., Wu, X., Betzig, E., and Hammer, J.A. (2016). Formin-generated actomyosin arcs propel T cell receptor microcluster movement at the immune synapse. *J. Cell Biol.* *215*, 383–399.
- Nordenfelt, P., Elliott, H.L., and Springer, T.A. (2016). Coordinated integrin activation by actin-dependent force during T-cell migration. *Nat. Commun.* *7*, 13119.
- Rak, G.D., Mace, E.M., Banerjee, P.P., Svitkina, T., and Orange, J.S. (2011). Natural killer cell lytic granule secretion occurs through a pervasive actin network at the immune synapse. *PLoS Biol.* *9*, e1001151.
- Ritter, A.T., Asano, Y., Stinchcombe, J.C., Dieckmann, N.M., Chen, B.C., Gawden-Bone, C., van Engelenburg, S., Legant, W., Gao, L., Davidson, M.W., et al. (2015). Actin depletion initiates events leading to granule secretion at the immunological synapse. *Immunity* *42*, 864–876.
- Sims, T.N., Soos, T.J., Xenias, H.S., Dubin-Thaler, B., Hofman, J.M., Waite, J.C., Cameron, T.O., Thomas, V.K., Varma, R., Wiggins, C.H., et al. (2007).

- Opposing effects of PKC $\theta$  and WASp on symmetry breaking and relocation of the immunological synapse. *Cell* 129, 773–785.
- Somersalo, K., Anikeeva, N., Sims, T.N., Thomas, V.K., Strong, R.K., Spies, T., Lebedeva, T., Sykulev, Y., and Dustin, M.L. (2004). Cytotoxic T lymphocytes form an antigen-independent ring junction. *J. Clin. Invest.* 113, 49–57.
- Stinchcombe, J.C., Bossi, G., Booth, S., and Griffiths, G.M. (2001). The immunological synapse of CTL contains a secretory domain and membrane bridges. *Immunity* 15, 751–761.
- Stinchcombe, J.C., Majorovits, E., Bossi, G., Fuller, S., and Griffiths, G.M. (2006). Centrosome polarization delivers secretory granules to the immunological synapse. *Nature* 443, 462–465.
- Tabdanov, E., Gondarenko, S., Kumari, S., Liapis, A., Dustin, M.L., Sheetz, M.P., Kam, L.C., and Iskratsch, T. (2015). Micropatterning of TCR and LFA-1 ligands reveals complementary effects on cytoskeleton mechanics in T cells. *Integr. Biol. (Camb.)* 7, 1272–1284.
- Theorell, J., Schlums, H., Chiang, S.C., Huang, T.Y., Tattermusch, A., Wood, S.M., and Bryceson, Y.T. (2011). Sensitive and viable quantification of inside-out signals for LFA-1 activation in human cytotoxic lymphocytes by flow cytometry. *J. Immunol. Methods* 366, 106–118.
- Trifari, S., Sitia, G., Aiuti, A., Scaramuzza, S., Marangoni, F., Guidotti, L.G., Martino, S., Saracco, P., Notarangelo, L.D., Roncarolo, M.G., and Dupré, L. (2006). Defective Th1 cytokine gene transcription in CD4+ and CD8+ T cells from Wiskott-Aldrich syndrome patients. *J. Immunol.* 177, 7451–7461.
- van de Linde, S., Löschberger, A., Klein, T., Heidbreder, M., Wolter, S., Heilemann, M., and Sauer, M. (2011). Direct stochastic optical reconstruction microscopy with standard fluorescent probes. *Nat. Protoc.* 6, 991–1009.
- Vasconcelos, Z., Müller, S., Guipouy, D., Yu, W., Christophe, C., Gadat, S., Valitutti, S., and Dupré, L. (2015). Individual human cytotoxic T lymphocytes exhibit intraclonal heterogeneity during sustained killing. *Cell Rep.* 11, 1474–1485.
- Wiedemann, A., Depoil, D., Faroudi, M., and Valitutti, S. (2006). Cytotoxic T lymphocytes kill multiple targets simultaneously via spatiotemporal uncoupling of lytic and stimulatory synapses. *Proc. Natl. Acad. Sci. USA* 103, 10985–10990.
- Yi, J., Wu, X.S., Crites, T., and Hammer, J.A., 3rd. (2012). Actin retrograde flow and actomyosin II arc contraction drive receptor cluster dynamics at the immunological synapse in Jurkat T cells. *Mol. Biol. Cell* 23, 834–852.
- Zhu, J., Luo, B.H., Xiao, T., Zhang, C., Nishida, N., and Springer, T.A. (2008). Structure of a complete integrin ectodomain in a physiologic resting state and activation and deactivation by applied forces. *Mol. Cell* 32, 849–861.